NASA-CR-199623

Grant Number NAG 5-2656
8/1/94-7/31/95

High Angular Resolution Far-Infrared and Submillimeter Mapping Survey of the Dust Cores Associated with Ultracompact HII Regions

Principal Investigator: T.G. Phillips
Division of Physics, Mathematics and Astronomy
California Institute of Technology

Final Report

The primary objective of the research funded under this grant has been to perform a high angular resolution mapping survey of the far-infrared and submillimeter continuum emission from the dust cocoons surrounding young, deeply embedded massive stars and the ultracompact H II regions they create. The high infrared, submillimeter, and radio luminosity makes the ultracompact H II regions ideal tracers of current high-mass star formation. Detailed investigations of their structure, evolution, and interaction with their parent molecular clouds are thus important for understanding the early evolutionary phases of massive main sequence stars, the nature of the dense molecular cores in which they form, and the relationship to coeval low-mass star formation.

During the duration of this grant we processed 73 fields surrounding ultracompact H II regions. For all these fields we obtained from IPAC Hires images, one square degree in size with 15″ pixels, at the wavelengths of 100, 60, 25, and 12 μm. The images were analyzed using Skyview. We performed aperture photometry on 126 sources which we identified as ultracompact H II regions. The list of these sources, together with their measured IRAS fluxes, and color temperatures between 60 and 100 μm are given in Table 1. This is the largest far-infrared sample of ultracompact H II regions compiled to date.

High angular resolution submillimeter observations of selected sources from Table 1 are a critical part of this project since they provide continuum fluxes at the wavelengths not covered by IRAS. The CSO bolometer camera (SHARC) was first tested in September 1995 and 350 and 450 μm observations of our target sources are currently under way. A 350 μm image of K 3–50 recently obtained with SHARC is shown in Figure 1. The image

provides an accurate measurement of the source size (16″) which is critical for detailed radiative transfer modeling.

For 13 sources we obtained 800 μm maps using the single channel CSO bolometer. For these sources we combined the far-infrared and submillimeter data to determine their spectral energy distributions. We fitted modified Planck functions to the observed fluxes in 4′ diameter apertures (e.g., Lis et al. 1991, ApJ, 380, 429). The observed fluxes and the fits are shown in Figure 2. Basic source parameters, including mean dust temperatures, emissivity law slopes, masses, luminosities, and the luminosity-to-mass ratios are summarized in Table 2. The spectra are characterized by shallow grain emissivity law, they are essentially diluted blackbody spectra. As discussed by Lis et al. (1991), the slopes derived from modified Planck function fits are not representative of the grain properties in the dust cores. However, the fits can be considered useful parameterization of the observed spectrum and thus provide a good estimate of the source luminosity.

The research described here is part of a Ph.D. thesis by T. Hunter and the results will be published upon completion of the submillimeter observations. Preliminary results will be presented at the AAS meeting in Austin, January 1996.

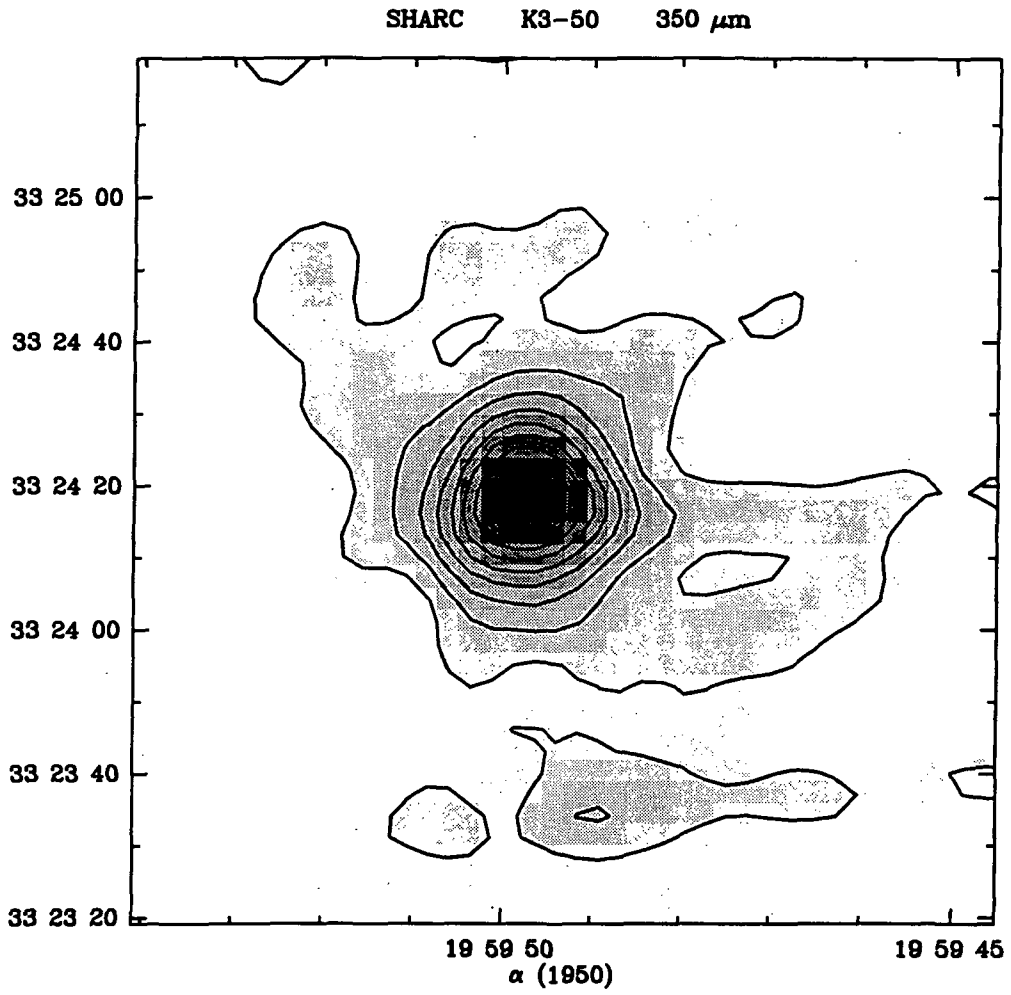

Figure 1: This 350 μm image of the ultracompact H II region K3–50 is one of the first images obtained with the SHARC camera. The contour levels are from 10 to 90% of the peak, in intervals of 10%. The high angular resolution of 13″ allows for accurate determination of the source size (16″ for K3–50). Observations of other sources from our target list are currently in progress.

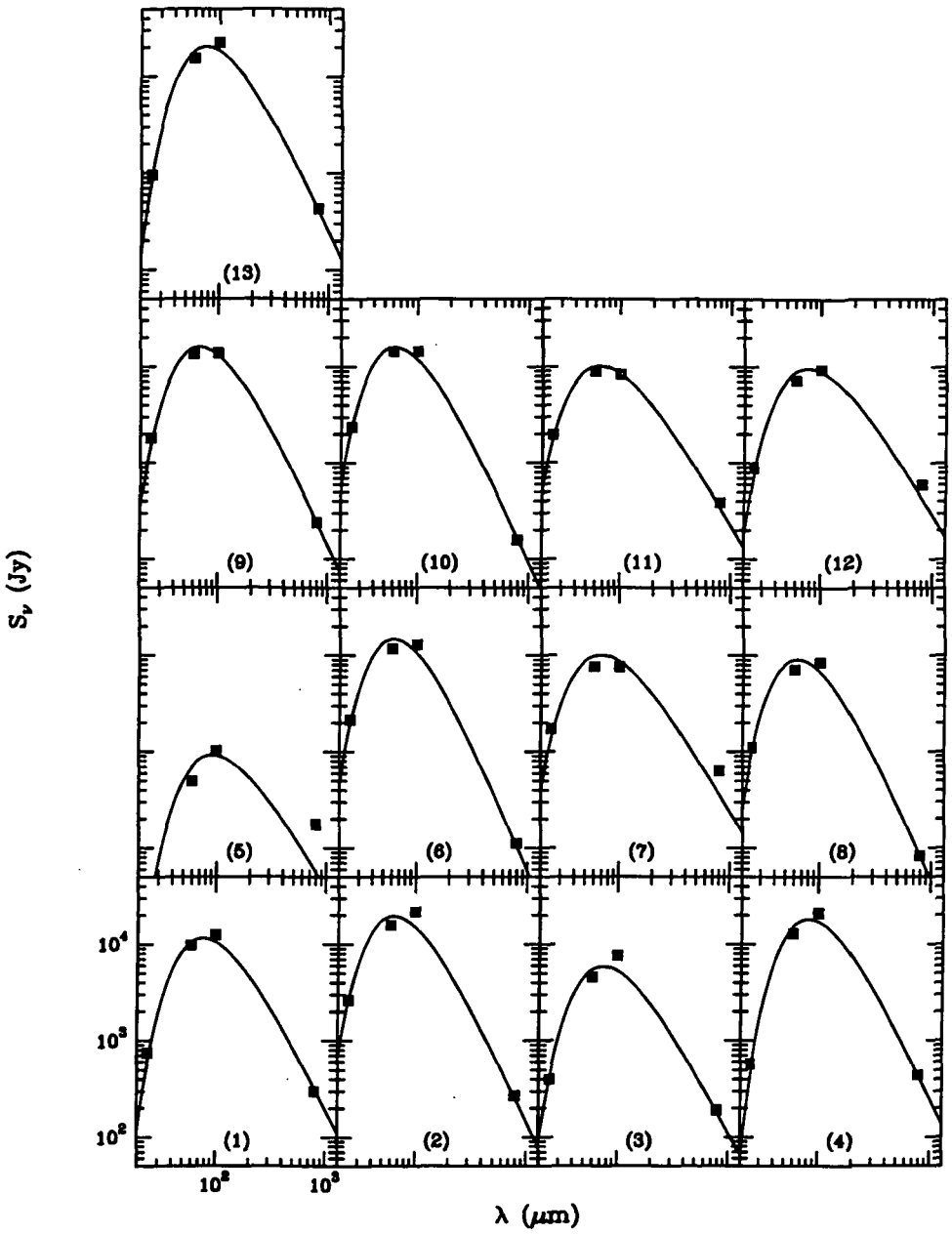

Figure 2: Spectra energy distributions of selected ultracompact H II regions for which 800 μm data have been obtained with the single channel CSO bolometer. The number given in each panel corresponds to that in column one of Table 2.

Table 1: UC HII Regions Analyzed with HiRes Processing

Source	Coordinates (1950.0) R.A.	Dec.	IRAS flux within 2′ radius (Jy) 100 μm	60 μm	25 μm	12 μm	T_{color} (K)	CSO 800 μm 1′	0.5′
G133.947+1.064	02h23m15.49s	61d38m57.0s	12569	9828	752	100	56.8	302	168
G138.30+1.56	02h57m36.20s	60d17m24.0s	1376	1002	291	55	53.2		
G140.909+0.197	03h03m31.30s	58d19m04.0s	1441	1267	504	73	60.4		
G206.543-16.35	05h39m09.30s	-1d57m40.0s	30326	18085	12485	1299	49.2		
MONR2IRS2	06h05m21.01s	-6d22m25.0s	20652	17649	5072	634	58.6		
G189.03+0.784	06h05m40.78s	21d31m27.9s	2924	2097	470	145	53.2		
G188.949+0.915	06h05m52.60s	21d38m58.0s	1745	1233	269	78	53.2		
G188.793+1.030	06h06m06.60s	21d51m13.0s	1288	1141	268	77	60.4		
G189.876+0.516	06h06m21.83s	20d40m04.9s	2592	2063	291	128	56.8		
IRAS06068+2030	06h06m53.88s	20d30m50.0s	1456	1240	208	102	58.6		
GGD12-15	06h08m24.10s	-6d11m08.0s	4975	3721	726	63	55.0		
G192.584-0.041	06h09m59.25s	18d00m16.0s	6247	4647	701	237	55.0		
NGC6334A	17h16m58.94s	-35d51m59.9s	26543	21731	3433	694	58.6		
NGC6334B	17h16m58.95s	-35d51m29.9s	22187	19198	3081	765	60.4		
NGC6334C	17h17m14.99s	-35d48m15.0s	22783	18924	6215	1325	58.6		
NGC6334D	17h17m27.31s	-35d47m30.0s	21220	19089	6201	1226	62.2		
NGC6334E	17h17m33.46s	-35d42m14.9s	23743	19177	2798	458	56.8		
NGC6334F	17h17m33.46s	-35d42m14.9s	24239	20944	2786	480	60.4		
G351.78-0.54	17h23m21.58s	-36d06m44.0s	17607	9720	392	86	46.0		
G1.13-0.11	17h45m33.34s	-28d00m29.0s	9320	4396	921	223	42.4		
G5.48-0.24	17h56m00.02s	-24d20m25.0s	2082	1537	260	47	53.2		
AFGL5425	17h56m52.91s	-23d45m11.6s	1950	1766	269	38	62.2		
G5.89-0.39	17h57m27.84s	-24d03m57.0s	21735	15872	2664	330	53.2	273	193
G6.55-0.01	17h57m46.38s	-23d20m25.6s	3604	2581	276	59	53.2		
AFGL5176S	17h58m53.22s	-23d58m40.9s	3146	2430	275	112	55.0		
G7.47+0.06	17h59m11.91s	-22d28m02.0s	3339	1499	227	108	42.4		
G8.14+0.23	18h00m00.21s	-21d48m15.0s	6451	5137	957	171	56.8		
G5.97-1.18	18h00m37.60s	-24d22m36.0s	10135	15407	5470	808	102.4		
G9.62+0.19	18h03m15.93s	-20d31m52.0s	7617	4620	403	63	47.8	193	103
G8.67-0.36	18h03m18.63s	-21d37m43.0s	5122	2338	198	33	42.4		
IRAS18035-2126	18h03m36.89s	-21d26m13.0s	916	730	79	30	56.8		
G10.47+0.03	18h05m41.09s	-19d52m25.6s	9895	4754	190	36	42.4		
G10.30-0.15	18h06m00.18s	-20d06m10.8s	11251	11119	2742	402	65.8		
G10.15-0.34	18h06m25.73s	-20d19m56.0s	26177	22250	6109	1013	58.6		
G9.876-0.750	18h07m21.44s	-20d45m52.0s	3541	1898	134	134	46.0		
G10.62-0.38	18h07m30.64s	-19d56m25.3s	21222	13024	582	83	47.8	444	288
G11.110-0.399	18h08m34.41s	-19d31m23.0s	3327	1443	271	105	40.6		
IRAS18089-1837	18h08m57.27s	-18d36m55.5s	1785	1545	283	57	60.4		
G12.21-0.10	18h09m45.82s	-18d25m26.0s	5125	3199	236	41	49.6		

Source	Coordinates (1950.0) R.A.	Dec.	IRAS flux within 2′ radius (Jy) 100 μm	60 μm	25 μm	12 μm	T_{color} (K)	CSO 800 μm 1′	0.5′
G12.68-0.18	18h11m00.19s	-18d01m48.9s	6542	3382	302	56	44.2		
G11.95-0.03	18h11m04.02s	-18d54m25.2s	4275	2399	274	10	46.0		
G13.19+0.04	18h11m10.59s	-17d29m18.8s	4417	3625	667	152	58.6		
G12.81-0.20	18h11m18.04s	-17d56m18.7s	31018	22339	3166	329	53.2		
G13.87+0.28	18h11m42.49s	-16d46m29.9s	5657	4402	753	141	55.0		
G12.91-0.26	18h11m44.30s	-17d53m03.2s	6425	3569	331	29	46.0		
G13.21-0.15	18h11m54.66s	-17d33m32.9s	2518	1134	84	14	42.4		
IRAS18134-1652	18h13m26.94s	-16d51m30.9s	4795	4140	648	175	60.4		
G10.841-2.592	18h16m13.01s	-20d48m48.0s	3802	3305	533	116	60.4		
G15.04-0.68	18h17m26.75s	-16d14m46.0s	19560	23149	4451	835	76.6		
G16.94-0.07	18h19m05.83s	-14d14m51.0s	2633	1149	207	109	40.6		
G18.146-0.284	18h22m13.26s	-13d17m34.0s	9859	9779	1798	390	65.8		
G18.302-0.391	18h22m52.29s	-13d12m03.8s	3355	2270	440	53	51.4		
G19.491+0.135	18h23m14.25s	-11d54m23.3s	2556	1465	158	36	46.0		
G19.07-0.27	18h23m58.90s	-12d28m07.0s	5785	4486	521	105	55.0		
G19.61-0.23	18h25m04.62s	-11d54m08.9s	1025	498	30	12	42.4	178	126
G20.08-0.14	18h26m12.93s	-11d26m07.9s	507	310	21	12	47.8		
G20.99+0.09	18h26m17.92s	-10d36m09.0s	1645	1237	130	31	55.0		
G23.70+0.17	18h31m08.73s	-8d09m38.9s	2841	2101	354	58	55.0		
G24.47+0.49	18h31m28.36s	-7d20m20.6s	7218	6052	1231	296	58.6		
G25.650+1.050	18h31m39.20s	-6d02m06.0s	2696	1097	220	82	40.6		
G23.96+0.15	18h31m42.06s	-7d57m08.8s	4053	3550	670	89	60.4		
G23.43-0.21	18h32m03.31s	-8d35m38.9s	9680	6022	572	130	49.6		
G23.87-0.12	18h32m30.56s	-8d09m08.7s	1922	1574	139	39	58.6		
IRAS18328-0735	18h32m50.03s	-7d35m51.0s	3848	2358	183	48	47.8		
IRAS18341-0727	18h34m09.70s	-7d27m20.5s	5297	3202	304	71	47.8		
G25.72+0.05	18h35m22.01s	-6d27m11.0s	4211	3006	367	78	53.2		
G25.38-0.18	18h35m29.06s	-6d49m11.0s	12834	13875	3493	506	71.2		
G26.54+0.42	18h35m34.30s	-5d32m20.0s	2180	1855	336	99	58.6		
G26.10-0.07	18h36m29.40s	-6d09m10.7s	1841	1287	112	30	53.2		
G27.28+0.15	18h37m54.86s	-5d00m29.9s	1963	1037	96	22	44.2		
G27.49+0.19	18h38m08.92s	-4d47m45.0s	2542	2001	219	48	56.8		
G28.198-0.050	18h40m19.89s	-4d16m59.9s	3953	2031	199	27	44.2		
IRAS18406-0338	18h40m37.96s	-3d38m30.0s	2872	2261	290	77	56.8		
G28.288-0.364	18h41m38.11s	-4d21m00.0s	3918	3456	977	101	60.4		
G28.60-0.36	18h42m10.18s	-4d04m29.8s	1968	1305	138	43	51.4		
G29.96-0.02	18h43m27.00s	-2d42m51.0s	12937	11832	2169	330	62.2	113	85
G30.53+0.02	18h44m24.98s	-2d10m32.0s	1503	1404	156	25	64.0		
G31.41+0.31	18h44m58.49s	-1d16m08.0s	2013	775	50	-6	38.8		
G30.78-0.02	18h45m01.01s	-1d58m32.0s	23611	25105	5750	1073	69.4		

Source	Coordinates (1950.0) R.A.	Dec.	IRAS flux within 2′ radius (Jy) 100 μm	60 μm	25 μm	12 μm	T_{color} (K)	CSO 800 μm 1′	0.5′
G31.28+0.06	18h45m37.50s	-1d29m38.0s	3638	1703	134	16	42.4		
G32.15+0.13	18h46m58.90s	-0d41m33.0s	1243	766	169	30	49.6		
G31.396-0.257	18h46m59.53s	-1d32m37.9s	3392	2297	311	53	51.4		
G32.80+0.19	18h47m18.00s	-0d22m45.0s	523	328	43	8	49.6		
G33.133-0.092	18h49m25.00s	0d11m00.0s	1839	1274	199	49	51.4		
G33.91+0.11	18h50m18.00s	0d51m45.0s	3165	1827	275	45	47.8		
G34.25+0.15	18h50m46.01s	1d11m00.0s	28752	18686	2291	342	49.6		
G35.57+0.06	18h53m31.01s	2d19m13.0s	3024	1397	186	87	42.4		
G35.578-0.030	18h53m52.02s	2d16m43.0s	4661	2990	323	106	49.6		
G37.55-0.11	18h57m46.42s	3d59m14.8s	3706	2288	275	92	49.6		
G35.200-1.741	18h59m14.10s	1d08m48.0s	15612	13366	2309	380	60.4		
G37.874-0.399	18h59m23.66s	4d08m30.0s	6266	4276	465	122	51.4		
G41.52+0.04	19h04m39.96s	7d34m15.0s	1585	763	132	69	42.4		
G41.71+0.11	19h04m49.04s	7d48m00.0s	1017	499	114	58	44.2		
G42.46-0.26	19h07m27.03s	8d14m33.0s	2941	1698	269	99	47.8		
W49N	19h07m49.59s	9d01m34.0s	30782	21796	3135	481	53.2		
G43.237-0.045	19h08m01.74s	9d01m19.0s	6219	3439	258	90	46.0		
G43.795-0.127	19h09m30.65s	9d30m40.4s	2761	1893	213	61	51.4		
G43.18-0.52	19h09m45.99s	8d47m10.6s	1903	1064	196	77	46.0		
G45.12+0.13	19h11m06.05s	10d48m29.7s	7603	7668	1742	350	67.6	641	221
G45.48+0.13	19h11m46.76s	11d07m15.0s	4562	3805	472	100	58.6		
G45.45+0.06	19h12m01.03s	11d04m00.0s	8539	7188	1120	184	58.6	83	51
G43.89+0.14	19h12m03.71s	9d17m25.6s	1873	1082	262	78	47.8		
IRAS19139+1113	19h14m00.31s	11d13m58.5s	1102	736	71	28	51.4		
G48.609+0.027	19h18m11.67s	13d49m38.0s	6956	5330	570	154	55.0		
G50.31+0.68	19h19m11.04s	15d38m28.8s	1214	774	149	57	49.6		
G53.605+0.046	19h28m09.60s	18d14m03.8s	2594	1372	142	98	44.2		
G54.10-0.06	19h29m31.82s	18d36m18.7s	3390	1848	261	101	46.0		
G60.884-0.128	19h44m14.80s	24d28m20.0s	5855	4585	820	159	56.8		
G61.48+0.09	19h44m40.79s	25d05m07.0s	13897	13575	1841	279	65.8	242	104
K3-50A	19h59m50.76s	33d24m21.9s	14386	14444	2391	516	67.6	159	97
G69.540-0.975	20h08m09.81s	31d22m41.0s	3516	1536	105	27	40.6		
G78.438+2.659	20h17m53.01s	40d47m06.0s	3864	3223	765	130	58.6		
G75.84+0.40	20h19m48.32s	37d21m28.8s	8376	9045	2004	699	71.2	389	137
G75.77+0.34	20h19m50.91s	37d16m28.9s	9418	7297	891	150	55.0	599	222
G76.18+0.10	20h22m05.56s	37d28m28.7s	2143	1474	189	50	51.4		
G76.38-0.621	20h25m33.79s	37d12m50.0s	14281	14353	3479	496	67.6		
G79.321+1.291	20h26m20.22s	40d42m15.0s	4972	4743	915	193	64.0		
G77.965-0.006	20h27m47.28s	38d51m16.0s	4251	3702	716	150	60.4		
G79.297+0.281	20h30m42.81s	40d06m04.0s	11715	14800	2103	398	82.0		

Source	Coordinates (1950.0) R.A.	Dec.	IRAS flux within 2′ radius (Jy) 100 μm	60 μm	25 μm	12 μm	T_{color} (K)	CSO 800 μm 1′	0.5′
G106.80+5.31	22h17m41.08s	63d03m42.0s	14064	12105	1641	347	60.4		
G109.87+2.11	22h54m17.77s	61d45m50.0s	22544	15473	961	27	51.4	433	205
G110.209+2.630	22h55m07.31s	62d21m40.0s	4068	3157	324	148	55.0		
NGC7538S	23h11m36.59s	61d11m50.0s	16882	13554	2554	432	56.8		
G111.612+0.374	23h13m19.24s	60d51m02.6s	3724	3168	779	112	58.6		
G111.282-0.663	23h13m54.59s	59d45m38.0s	2977	2286	402	98	55.0		
IRAS23139+5939	23h13m58.54s	59d39m23.0s	1208	624	111	45	44.2		

Table 3: UC HII Regions Observed at 800 μm at CSO

Source Number	Source Name	Temp. (K)	Spectral Index (β)	Dist. (kpc)	Luminosity (10^6 $L_\odot$)	Mass ($M_\odot$)	Lum./Mass ($L_\odot$ / $M_\odot$)
1	G133.947+1.064	59.4	0.30	3.0	1.55×10^6	5.85×10^2	2.65×10^3
2	G5.89-0.39	67.0	0.50	2.6	3.01×10^6	4.40×10^2	2.65×10^3
3	G9.62+0.19	63.2	0.20	5.7	8.25×10^5	9.22×10^2	8.94×10^2
4	G10.62-0.38	51.8	0.50	6.5	2.19×10^5	6.29×10^3	3.47×10^2
5	G19.61-0.23	55.6	0.00	4.5	1.10×10^5	1.44×10^2	7.61×10^2
6	G29.96-0.02	63.2	0.80	9.0	2.23×10^6	4.00×10^3	5.58×10^2
7	G45.12+0.13	75.6	0.00	8.4	1.61×10^6	2.24×10^3	7.17×10^2
8	G45.45+0.06	63.2	0.70	9.7	1.36×10^6	1.17×10^3	1.16×10^3
9	G61.48+0.09	63.2	0.50	2.0	2.33×10^6	2.60×10^2	8.94×10^3
10	K3-50A	67.0	0.60	8.0	2.48×10^6	3.16×10^3	7.85×10^2
11	G75.84+0.40	78.4	0.00	5.5	1.70×10^6	8.59×10^2	1.98×10^3
12	G75.77+0.34	67.0	0.00	5.6	1.39×10^6	1.35×10^3	1.03×10^3
13	G109.87+2.11	55.6	0.50	0.7	2.62×10^6	6.36×10^1	4.11×10^4